



PAPER

Thermodynamics of wetting, prewetting and surface phase transitions with surface binding




OPEN ACCESS

RECEIVED
9 July 2021REVISED
5 October 2021ACCEPTED FOR PUBLICATION
21 October 2021PUBLISHED
1 December 2021

Original content from
this work may be used
under the terms of the
[Creative Commons
Attribution 4.0 licence](https://creativecommons.org/licenses/by/4.0/).

Any further distribution
of this work must
maintain attribution to
the author(s) and the
title of the work, journal
citation and DOI.



Xueping Zhao^{1,2}, Giacomo Bartolucci^{1,2}, Alf Honigmann^{2,3} , Frank Jülicher^{1,2,4,*} 
and Christoph A Weber^{1,2,*} 

¹ Max Planck Institute for the Physics of Complex Systems, Nöthnitzer Strasse 38, 01187 Dresden, Germany

² Center for Systems Biology Dresden, Pfotenhauerstrasse 108, 01307 Dresden, Germany

³ Max Planck Institute of Molecular Cell Biology and Genetics, Pfotenhauerstrasse 108, 01307 Dresden, Germany

⁴ Cluster of Excellence Physics of Life, TU Dresden, 01062 Dresden, Germany

* Authors to whom any correspondence should be addressed.

E-mail: julicher@pks.mpg.de and christoph.weber@physik.uni-augsburg.de

Keywords: surface phase transitions, thermodynamics of wetting and prewetting, surface binding

Abstract

In living cells, protein-rich condensates can wet the cell membrane and surfaces of membrane-bound organelles. Interestingly, many phase-separating proteins also bind to membranes leading to a molecular layer of bound molecules. Here we investigate how binding to membranes affects wetting, prewetting and surface phase transitions. We derive a thermodynamic theory for a three-dimensional bulk in the presence of a two-dimensional, flat membrane. At phase coexistence, we find that membrane binding facilitates complete wetting and thus lowers the wetting angle. Moreover, below the saturation concentration, binding facilitates the formation of a thick layer at the membrane and thereby shifts the prewetting phase transition far below the saturation concentration. The distinction between bound and unbound molecules near the surface leads to a large variety of surface states and complex surface phase diagrams with a rich topology of phase transitions. Our work suggests that surface phase transitions combined with molecular binding represent a versatile mechanism to control the formation of protein-rich domains at intra-cellular surfaces.

1. Introduction

Surfaces introduce a new level of complexity, as Wolfgang Pauli alluded to in his famous quote: ‘God made the bulk; surfaces were invented by the devil’ [1]. This complexity is ubiquitous in nature since surfaces are key determinants in many biological systems. A paradigm are living cells which are surrounded by a membrane and that contain intricate organelles enclosed by membranes. While a major function of membranes is to compartmentalize biochemical reactions in cells, the interplay between membranes and the cellular bulk is crucial for many biological processes. Examples are sensing and signaling, endocytosis or asymmetric cell division. In addition to membranes, cells use protein-rich condensates to organize intra-cellular space. Such condensates coexist with the cellular environment and share hallmark properties of physical droplets [2–6]. Interestingly, protein condensates can adhere to intracellular surfaces and membrane-bound organelles [2, 7, 8], which resemble condensates wetted on surfaces. These observations indicate that phase-separating proteins in living cells not only phase-separate in the bulk but can also undergo phase transitions related to the membrane surface.

The theory of surface phase transitions was developed by Cahn [9]. In this seminal work, he discussed the graphical construction for wetting transitions but also showed the existence of prewetting transitions. In the same year, Ebner and Saam reported wetting and prewetting transitions using density-functional theory [10]. The wetting transition separates the regime of complete wetting and partial wetting, where the interface of wetting droplets exhibits a contact angle with respect to the surface [9, 11–18]. While wetting solely occurs inside the binodal of the corresponding bulk phase diagram (coexistence domain), prewetting

phase transitions take place in the undersaturated regime where droplets shrink and disappear in the bulk. Inside the prewetting regime of the phase diagram, a three-dimensional layer forms close to the surface which we refer to as the ‘thick layer’. The layer thickness can be quantified by the excess surface concentration which serves as an order parameter for the wetting and prewetting transitions. Crossing the prewetting transition, e.g. by lowering the bulk concentration, the excess surface concentration (order parameter) decreases discontinuously to a lower value and molecules accumulate only very weakly at the surface, forming the ‘thin layer’. The close vicinity of the prewetting transition line and the binodal for many polymeric systems was an experimental challenge to distinguish bulk and phase transitions at surfaces [19–21].

Many of the phase-separating proteins have molecular domains by which they can bind to membranes [22–24]. Reversible membrane binding of proteins in the presence of chemical feedback is known to give rise to reaction-diffusion patterns on membranes [25–27]. In contrast to wetted or prewetted states, these patterns are comprised of mono-layered, two-dimensional domains of specific protein composition leading to a spatially organized membrane. Wetting or prewetting can however give rise to surface condensates that are three-dimensional. Such condensates can serve as hubs for down-stream assembly processes at membrane surfaces [8, 24, 28]. Prewetting could also serve as a mechanism for the formation of proteins condensates on DNA strands [29, 30] and thus play a role in chromatin organization. In summary, condensation at surfaces such as membranes or biofilaments appears as a key principle of spatial organization of biological surfaces [31]. However, a general thermodynamic theory that explores how protein binding to biological surfaces affects surface condensation is lacking.

In this work, we study the interplay between wetting, prewetting and surface phase transitions coupled via binding of molecules between bulk and membrane surface. We propose a general thermodynamic free energy that captures the molecular interactions in the three-dimensional bulk and a two-dimensional, flat surface. Using this free energy, we determine the phase diagrams for wetting and prewetting at thermodynamic equilibrium. By varying the parameters that describe surface binding of molecules, we find phase diagrams of variable complexity and topology which exhibit transitions between a rich set of thermodynamic surface states (figure 8). We find that binding can enlarge the regime of wetting and prewetting, and can move the prewetting transition to lower bulk concentrations. Another finding is that binding can give rise to prewetted states not only below the critical point but also in the absence of bulk phase separation.

2. Thermodynamics of phase separation with membrane binding

We consider a liquid solution where solute molecules can bind to specific sites on a two-dimensional, flat membrane at $z = 0$. The volume fraction of molecules in the bulk is denoted by $\phi(x, y, z)$, the density of molecules bound to the membrane is described by the area fraction $\phi_m(x, y)$. During binding and unbinding events molecules transition between the solute state and the surface bound state according to



Here we study how phase separation in bulk and surface affects wetting and prewetting transitions by surface binding (figures 1(a)–(c)). To this end, we consider a bulk binary mixture of volume V which is composed of solute molecules and solvent. The free energy contains contributions from the bulk $f_b(\phi)$, the membrane $f_m(\phi_m)$ and coupling free energy between them, $J(\phi|_0, \phi_m)$:

$$F[\phi, \phi_m] = \int_V d^3x \left[f_b(\phi) + \frac{1}{2} \kappa |\nabla \phi|^2 \right] + \int_m d^2x \left[f_m(\phi_m) + \frac{1}{2} \kappa_m |\nabla_{\parallel} \phi_m|^2 + J(\phi|_0, \phi_m) \right], \quad (2)$$

where $\phi|_0$ is the bulk volume fraction at the membrane surface. Moreover, κ and κ_m characterize the corresponding free energy penalties for gradients in bulk and membrane, respectively, and $\nabla_{\parallel} = (\partial_x, \partial_y)$ denotes the gradient vector in the membrane plane. From equation (2) we can define the local chemical potential $\mu = \nu_b \delta F / \delta \phi$ and $\mu_m = \nu_m \delta F / \delta \phi_m$, where ν_b and ν_m denote the molecular volume and the molecular surface area of the molecules, respectively.

2.1. Thermodynamics of a semi-infinite system

We consider a semi-infinite, thermodynamic system with the membrane at $z = 0$. Systems that are homogeneous in the x – y plane become effectively one-dimensional with a bulk volume fraction $\phi(z)$

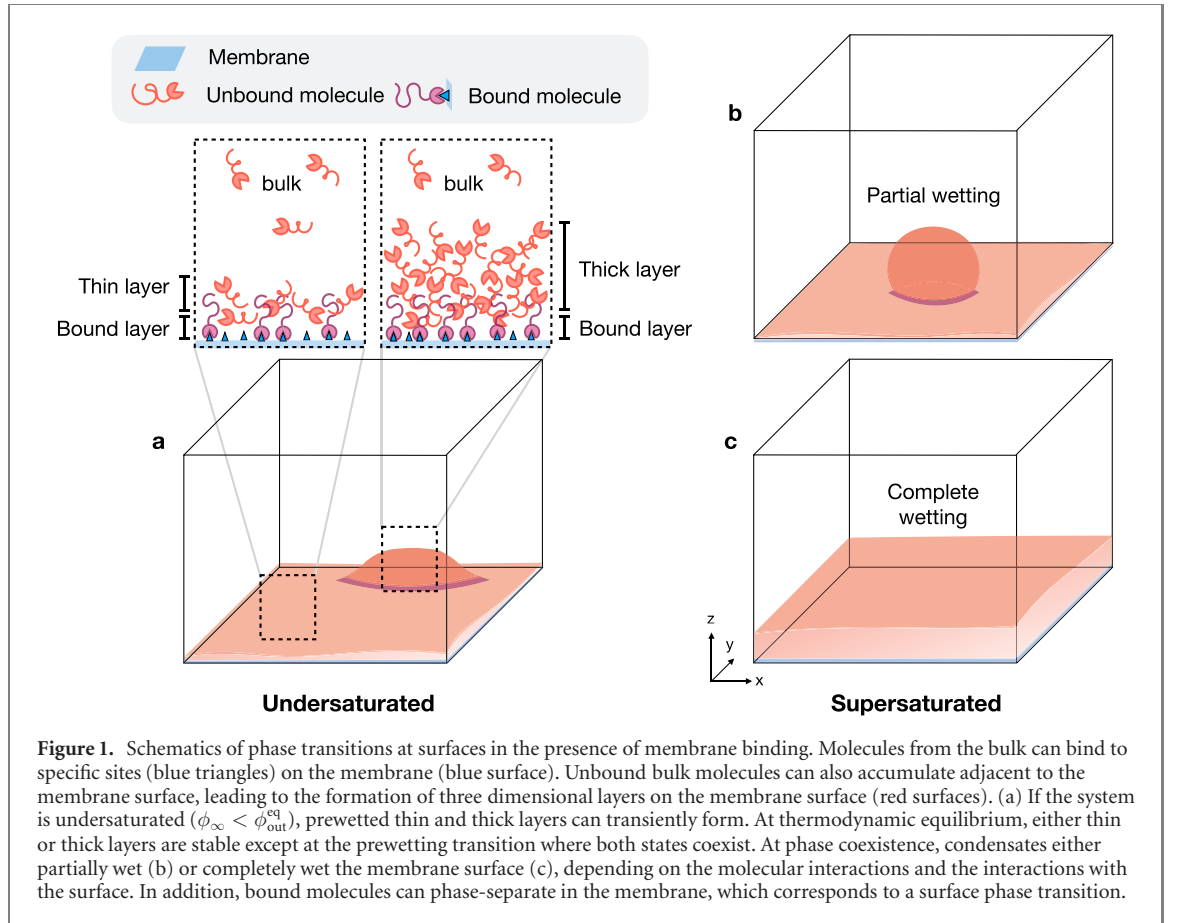


Figure 1. Schematics of phase transitions at surfaces in the presence of membrane binding. Molecules from the bulk can bind to specific sites (blue triangles) on the membrane (blue surface). Unbound bulk molecules can also accumulate adjacent to the membrane surface, leading to the formation of three dimensional layers on the membrane surface (red surfaces). (a) If the system is undersaturated ($\phi_\infty < \phi_{out}^{eq}$), prewetted thin and thick layers can transiently form. At thermodynamic equilibrium, either thin or thick layers are stable except at the prewetting transition where both states coexist. At phase coexistence, condensates either partially wet (b) or completely wet the membrane surface (c), depending on the molecular interactions and the interactions with the surface. In addition, bound molecules can phase-separate in the membrane, which corresponds to a surface phase transition.

changing along the z -direction with $z \in [0, \infty)$. The corresponding Helmholtz surface free energy functional reads

$$f_s[\phi, \phi_m] = \int_0^\infty dz \left[f_b(\phi) - f_b(\phi_\infty) + \frac{1}{2} \kappa |\partial_z \phi|^2 \right] + f_m(\phi_m) + J(\phi|_0, \phi_m), \quad (3)$$

where $\phi_\infty = \phi(z \rightarrow \infty)$ is the bulk volume fraction far away the surface with the corresponding the external chemical potential $\mu_\infty = df_b/d\phi|_{\phi=\phi_\infty}$. We also define the excess surface concentration

$$c_s = \int_0^\infty dz \left[\frac{1}{\nu_b} (\phi(z) - \phi_\infty) \right]. \quad (4)$$

We obtain the surface free energy $f_s(c_s, \phi_m)$ when evaluating f_s for the profile $\phi(z)$ that minimizes equation (3) for fixed c_s and ϕ_m , and with ϕ_∞ given far away from the membrane. The surface free energy $f_s(c_s, \phi_m)$ depends on the membrane area fraction ϕ_m and the excess surface concentration c_s and has units of an energy per area. The chemical potentials in bulk and membrane can now be expressed as

$$\mu = \frac{\partial f_s}{\partial c_s}, \quad (5a)$$

$$\mu_m = \nu_m \frac{\partial f_s}{\partial \phi_m}. \quad (5b)$$

We can use a Legendre transformation to define the Gibbs surface free energy which is the surface thermodynamic potential in the ensemble where the chemical potentials are fixed:

$$\gamma_s(\mu, \mu_m) = f_s(c_s, \phi_m) - \mu c_s - \mu_m \frac{\phi_m}{\nu_m}. \quad (6)$$

The conjugate variables to each of the chemical potentials μ and μ_m are the excess surface concentration c_s and the area fraction ϕ_m ,

$$c_s = -\frac{\partial\gamma_s}{\partial\mu}, \quad (7a)$$

$$\phi_m = -\nu_m \frac{\partial\gamma_s}{\partial\mu_m}. \quad (7b)$$

In the following, both variables serve as order parameters for wetting, prewetting and surface phase transitions. In particular, c_s characterizes the bulk layer adjacent to the surface while ϕ_m describes the state of the membrane.

2.2. Free energy minimization in a semi-infinite system

We determine the equilibrium states via minimization of the Helmholtz surface free energy functional $f_s[\phi, \phi_m]$, while keeping c_s and ϕ_m fixed. This is achieved by minimizing the Gibbs surface free energy functional $\gamma_s[\phi, \phi_m] = f_s[\phi, \phi_m] - \mu c_s - \mu_m \phi_m / \nu_m$, where μ and μ_m act as Lagrange multipliers to impose fixed c_s and ϕ_m , respectively. At this minimum, $\delta\gamma_s = 0$, where

$$\begin{aligned} \delta\gamma_s[\phi, \phi_m] = & \int_0^\infty dz \left[\left(\frac{\partial f_b}{\partial\phi} - \frac{1}{\nu_b} \mu - \kappa \partial_z^2 \phi \right) \delta\phi \right] + \kappa \frac{d\phi}{dz} \delta\phi|_0^\infty \\ & + \left[\frac{\partial f_m}{\partial\phi_m} + \frac{\partial J(\phi|_0, \phi_m)}{\partial\phi_m} - \frac{1}{\nu_m} \mu_m \right] \delta\phi_m + \frac{\partial J(\phi|_0, \phi_m)}{\partial\phi|_0} \delta\phi|_0 \end{aligned} \quad (8)$$

is the functional variation of the Gibbs free energy functional $\gamma_s[\phi, \phi_m]$. This leads to the equilibrium conditions:

$$\frac{\partial f_b}{\partial\phi} - \frac{1}{\nu_b} \mu_\infty - \kappa \partial_z^2 \phi = 0, \quad z \in [0, \infty), \quad (9a)$$

$$\phi(z)|_{z \rightarrow \infty} = \phi_\infty, \quad (9b)$$

$$-\kappa \frac{d\phi}{dz} \Big|_{z=0} + \frac{\partial J(\phi, \phi_m)}{\partial\phi} \Big|_{z=0} = 0, \quad (9c)$$

$$\frac{\partial f_m}{\partial\phi_m} + \frac{\partial J(\phi, \phi_m)}{\partial\phi_m} \Big|_{z=0} - \frac{1}{\nu_m} \mu_\infty = 0, \quad (9d)$$

where we used that binding between membrane and bulk (equation (1)) is at thermodynamic equilibrium: $\mu_m = \mu_\infty$, where μ_∞ denotes the chemical potential of the reservoir at $z \rightarrow \infty$. Note that at thermodynamic equilibrium, the gradient of the bulk profile $\phi(z)$ vanishes far away from the membrane, $d\phi/dz|_{z \rightarrow \infty} = 0$.

By integration over the bulk (see appendix A) and using equation (9b), we can rewrite equation (9):

$$\partial_z \phi \pm \sqrt{\frac{2}{\kappa} W(\phi)} = 0, \quad z \in [0, \infty), \quad (10a)$$

$$\sqrt{2\kappa W(\phi|_0)} \pm \frac{\partial J(\phi, \phi_m)}{\partial\phi} \Big|_0 = 0, \quad (10b)$$

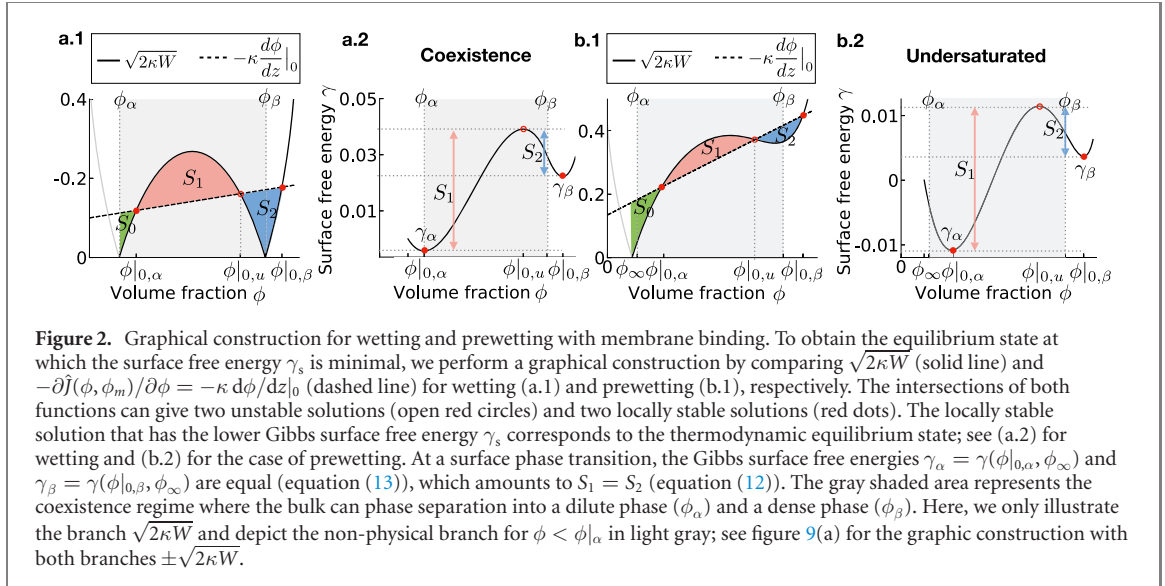
$$\frac{\partial f_m}{\partial\phi_m} + \frac{\partial J(\phi, \phi_m)}{\partial\phi_m} \Big|_{z=0} - \frac{1}{\nu_m} \mu_\infty = 0, \quad (10c)$$

where $W(\phi)V$ is the free energy needed to create a uniform fluid volume V of composition ϕ from the reservoir of composition ϕ_∞ [9],

$$W(\phi) = f_b(\phi) - \mu_\infty \frac{1}{\nu_b} \phi + \Pi_\infty, \quad (10d)$$

and $\Pi_\infty = -f_b(\phi_\infty) + \mu_\infty \phi_\infty / \nu_b$ is the osmotic pressure of the particle bath at $z \rightarrow \infty$. Note that \pm indicates that, in general, we need to solve equations (10a) and (10b) with both signs to obtain all solutions of equation (9) (for a detailed discussion see Appendix A and figure 9(a)).

We use equations (10b) and (10c) to obtain the membrane area fraction ϕ_m and bulk volume fraction at the surface $\phi|_0$. The spatial bulk profile $\phi(z)$ then follows from equation (10a). Using this profile we can compute the excess surface concentration c_s (equation (4)). The thermodynamic control parameter is the chemical potential of the reservoir, μ_∞ . We also use the volume fraction of the reservoir ϕ_∞ as control parameter, which is equivalent to the average volume fraction $\bar{\phi}$ in the thermodynamic limit. We calculate



the surface phase diagrams as a function of $\bar{\phi}$ and parameters characterising the interactions among the molecules (see section 3.1).

2.3. Surface phase diagrams obtained via graphical construction

The transition lines separating different thermodynamic states at the surface can also be obtained via a graphical construction. Using equation (10a), we can rewrite the Gibbs surface free energy functional (equation (6) with f_s given by equation (3)) leading to

$$\gamma(\phi, \phi_\infty) = \int_{\phi_\infty}^{\phi} d\phi' \left[\pm\sqrt{2\kappa W(\phi')} + \frac{\partial\hat{J}}{\partial\phi'} \right] + \hat{J}(\phi_\infty, \phi_m), \quad (11)$$

where $\hat{J}(\phi, \phi_m) = J(\phi, \phi_m) + f_m(\phi_m) - \nu_m^{-1}\mu_\infty\phi_m$, with $\partial\hat{J}/\partial\phi_m = 0$ (see equation (10c)), and $\phi|_0$ and ϕ_m are determined by equation (10b). The integral term in equation (11) corresponds to the area between $\pm\sqrt{2\kappa W(\phi)}$ and $-\partial\hat{J}/\partial\phi$ and can be illustrated graphically (see colored areas in figure 2).

Now we can define the Gibbs surface potential as $\gamma_s = \gamma(\phi|_0, \phi_\infty)$. Local extrema of the Gibbs surface potential correspond to the intersection points between $\pm\sqrt{2\kappa W(\phi)}$ and $-\partial\hat{J}/\partial\phi$. There can be two local minima, $\gamma_\alpha = \gamma_s(\phi|_{0,\alpha}, \phi_\infty)$ and $\gamma_\beta = \gamma_s(\phi|_{0,\beta}, \phi_\infty)$, and the intermediate local maximum is denoted by $\gamma_u = \gamma_s(\phi|_{0,u}, \phi_\infty)$. The differences between these extremal values of the Gibbs surface potential can be expressed as the areas between $\pm\sqrt{2\kappa W(\phi)}$ and $-\partial\hat{J}/\partial\phi$. Specifically, $\gamma_\alpha = -S_0 + \hat{J}(\phi_\infty, \phi_m)$, $\gamma_u = -S_0 + S_1 + \hat{J}(\phi_\infty, \phi_m)$ and $\gamma_\beta = -S_0 + S_1 - S_2 + \hat{J}(\phi_\infty, \phi_m)$ (see colored domains in figures 2(a.1) and (b.1)). Thus, we find that the surface free energies at the minima are related by

$$\gamma_\alpha = \gamma_\beta + S_1 - S_2. \quad (12)$$

At the prewetting and wetting transition lines, the Gibbs surface free energies of both states α and β are equal:

$$\gamma_\alpha = \gamma_\beta, \quad (13)$$

which implies, using equation (12), that $S_1 = S_2$ at the transition line. This defines the graphical construction and determines the value of the control parameter, e.g. $\bar{\phi}$, at which the transition occurs. The minimized surface free energies exhibit a kink at both the wetting and prewetting transition (characterized by c_s) and the surface phase transition (characterized by ϕ_m). However, due to the coupling between bulk and membrane, both order parameters, area fraction ϕ_m and the excess surface concentration c_s , in general change discontinuously at each of the transitions.

If the average volume fraction of the system $\bar{\phi}$ is within the domain of phase coexistence, i.e. $\phi_\alpha < \bar{\phi} < \phi_\beta$ for a certain range of interaction parameters, the homogeneous mixture is unstable and phase-separates into a dilute and a dense phase, with respective equilibrium values ϕ_α and ϕ_β . Based on the definition of the Gibbs surface free energy density $\gamma_s = \gamma(\phi|_0, \phi_\infty)$ (equation (11)), we identify the surface

tensions between the membrane and the dilute phase $\gamma_{s,\alpha}$, between the membrane and the dense phase $\gamma_{s,\beta}$, and between the dilute and dense phase $\gamma_{\alpha,\beta}$, as follows:

$$\gamma_{s,\alpha} = \gamma(\phi|_{0,\alpha}, \phi_\alpha), \quad (14a)$$

$$\gamma_{s,\beta} = \gamma(\phi|_{0,\beta}, \phi_\beta), \quad (14b)$$

$$\gamma_{\alpha,\beta} = \int_{\phi_\alpha}^{\phi_\beta} d\phi \sqrt{2\kappa W}. \quad (14c)$$

These equations satisfy the Young–Dupré law, $\gamma_{s,\alpha} = \gamma_{s,\beta} + \gamma_{\alpha,\beta} \cos(\theta)$, which defines the contact angle. The wetting transition is characterized by equal Gibbs surface free energy of the partially wetted state $\gamma_\alpha = \gamma_{s,\alpha}$, and the completely wetted state $\gamma_\beta = \gamma_{s,\beta} + \gamma_{\alpha,\beta}$ (equation (13)), corresponding to zero contact angle, $\theta = 0$.

If the average volume fraction of the system $\bar{\phi}$ is outside the domain of phase coexistence, e.g. $\bar{\phi} < \phi_\alpha$ or $\bar{\phi} > \phi_\beta$, there can still be two surface states corresponding to two local minima of the Gibbs surface free energy as can be seen from the graphical construction, figure 2(b.2). When equation (13) is satisfied and the two free energy minima are equal, a phase transition occurs. Due to the coupling between bulk and membrane, the corresponding phase transition in general shares the characteristics of a prewetting transition with a discontinuous behavior in the excess surface concentration c_s and a surface phase transition with discontinuous behavior of the membrane area fraction ϕ_m .

2.4. Bulk and membrane free energies

To calculate the surface phase diagram using the graphical construction as well as the profile $\phi(z)$ at thermodynamic equilibrium, we consider the following free energy for the bulk (b) and the membrane (m):

$$f_b(\phi) = \frac{k_B T}{\nu} \left[\frac{1}{n_b} \phi \ln \phi + (1 - \phi) \ln(1 - \phi) + \chi_b \phi(1 - \phi) \right], \quad (15a)$$

$$f_m(\phi_m) = \frac{k_B T}{\tilde{\nu}} \left[\frac{1}{n_m} \phi_m \ln \phi_m + (1 - \phi_m) \ln(1 - \phi_m) + \chi_m \phi_m(1 - \phi_m) + \omega_m \phi_m \right], \quad (15b)$$

where ν and $\tilde{\nu}$ are the solvent molecular volume and solvent molecular surface area, respectively. Bulk molecules have a molecular volume of $\nu_b = \nu n_b$, while bound molecules occupy an area of $\nu_m = \tilde{\nu} n_m$. Here, n_b and n_m are the fractions of molecular volumes or surface areas of the molecules compared to the solvent, respectively. Molecular interactions among molecules in the bulk and membrane are described by the interaction parameters χ_b and χ_m , respectively. Both parameters are in general different since molecular interactions can change upon binding. The internal free energy difference between membrane molecules and bulk molecules is denoted by ω_m .

The coupling free energy between bulk and membrane reads:

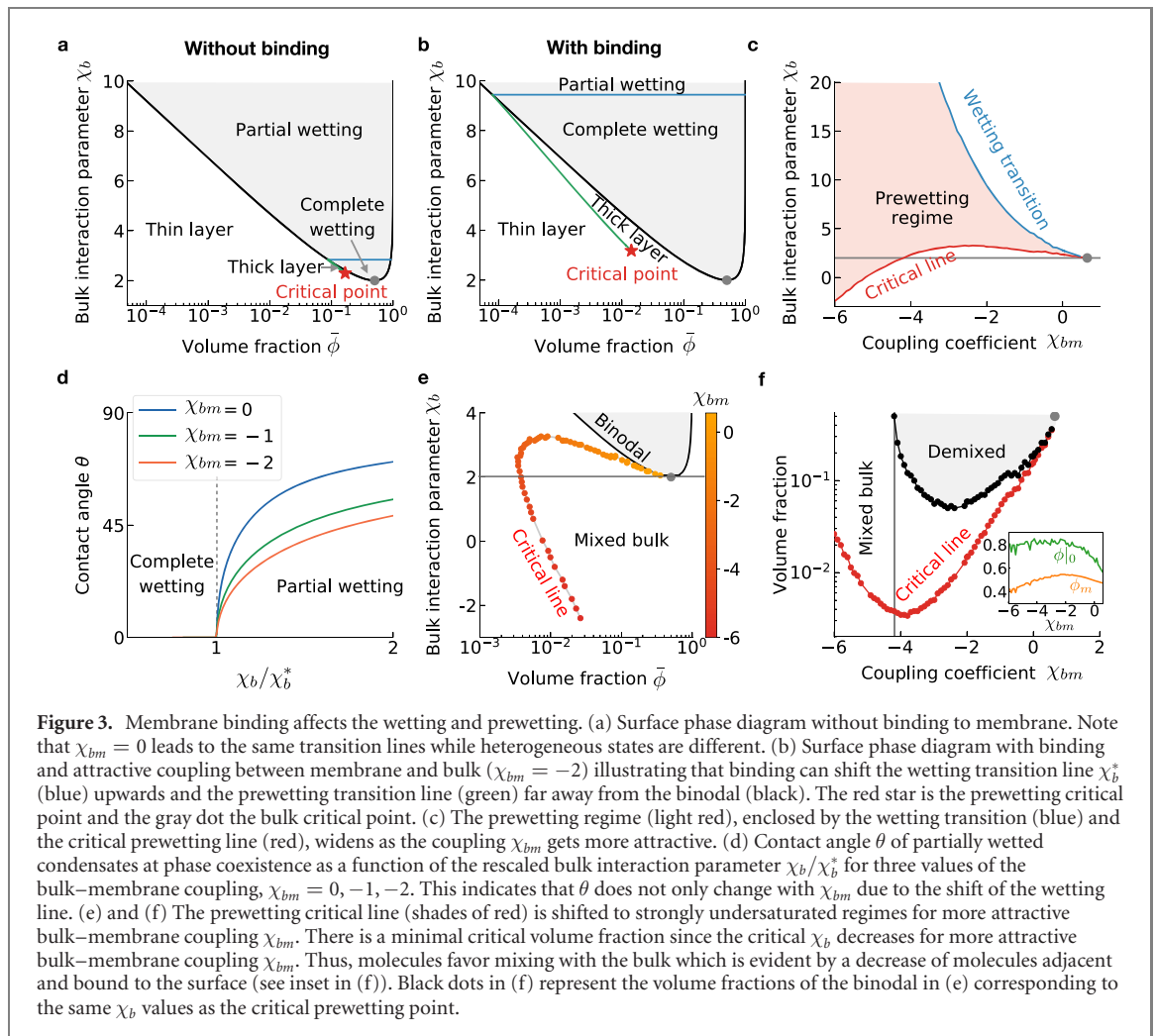
$$J(\phi, \phi_m) = \frac{k_B T}{\tilde{\nu}} [\omega_b \phi + \chi_{bb} \phi^2 + \chi_{bm} \phi \phi_m], \quad (15c)$$

where ω_b is the internal free energy of a bulk molecule at the surface. When the surface is attractive for molecules in the bulk, $\omega_b < 0$. The interaction parameter χ_{bb} accounts for enhanced interactions by accumulating bulk molecules at the surfaces. Note that in previous work, wetting, prewetting and surface phase transitions were studied using the surface interaction parameters ω_b and χ_{bb} [9, 11]; (see Appendix C for comparison of our model with reference [11]). In our model, we additionally account for the coupling between bulk and membrane surface via the parameter χ_{bm} . This parameter characterizes the interactions between membrane-bound molecules and bulk molecules at the surface. The term $\chi_{bm} \phi_m$ can also be considered as a further contribution to the internal free energy ω_b due to molecules that are bound to the surface.

3. Effects of membrane binding on wetting, prewetting and surface phase transitions

3.1. Wetting and prewetting without phase separation in the membrane

Here, we first study how binding affects wetting and prewetting for cases where the surface free energy f_m of membrane cannot give rise to coexisting phases in the membrane ($\chi_m = -4$). For simplicity, the membrane insertion energy ω_m is set to zero. Moreover, we consider an internal free energy corresponding to attractive interactions between membrane and bulk, $\omega_b = -0.3$, and no enhanced interactions, $\chi_{bb} = 0$. The effects of binding is studied for varying the bulk interaction parameter χ_b , the bulk volume fraction ϕ_∞ , and the



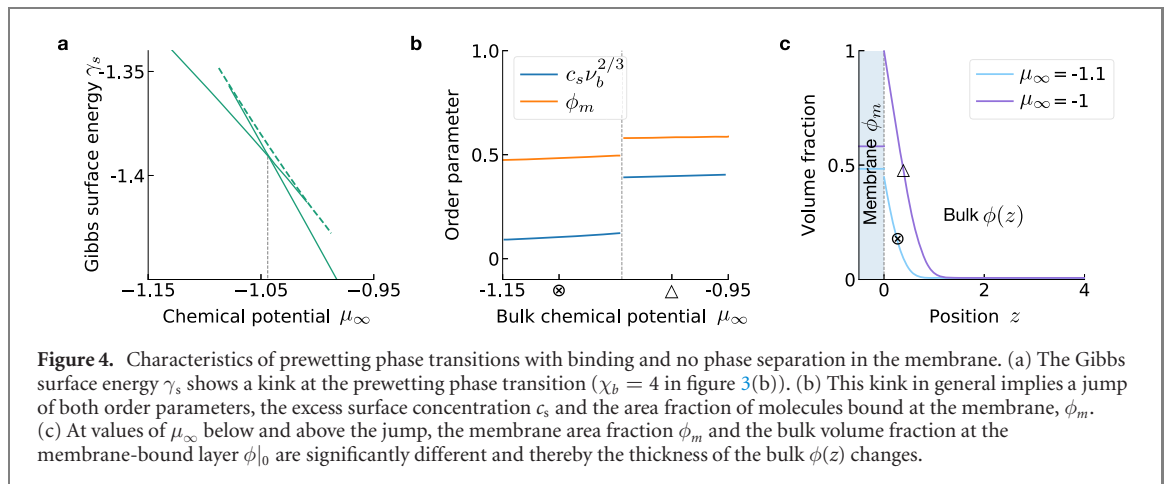
coupling parameter between bulk and membrane, χ_{bm} . We compare the corresponding results to the same system in the absence of membrane binding, $\chi_{bm} = 0$. Please note that the transition line for our model without binding ($\phi_m = 0$) is the same as in the case with binding and vanishing bulk–membrane coupling ($\chi_{bm} = 0$). The corresponding surface phase diagram is shown in figure 3(a). This diagram depicts the domains with partially and completely wetted states separated by the wetting transition (blue line). It also shows the prewetting line (green line) separating thin and thick layer states. At both transitions, the excess surface concentration c_s is discontinuous. The red star represents the prewetting critical point where thin and thick layer state become indistinguishable. In Appendix B, we give the condition for the critical point.

3.1.1. Membrane binding favors complete wetting and reduces the contact angle

Binding to the membrane has significant effects on the wetting transition (compare figures 3(a) and (b)). In particular, when increasing the attraction between the bulk and the membrane by reducing χ_{bm} , complete wetting is favored. This trend is evident in an upshift of the bulk interaction parameter at which the wetting transition occurs, χ_b^* , with decreasing coupling parameter χ_{bm} (blue line in figure 3(c)). Note that at the wetting transition, there is a kink in the surface free energies (equation (13)) and the excess surface concentration c_s and membrane area fraction ϕ_m jumps. In addition, for more attractive couplings between membrane and bulk, the wetting angle decreases (colored lines in figure 3(d)). This behavior is not only due to the shift of the wetting transition $\chi_b^*(\chi_{bm})$. Since the coupling is a second order term that describes the interactions between membrane and bulk, the trend of decreasing wetting angle with more attractive χ_{bm} persists even after rescaling χ_b by the wetting transition χ_b^* .

3.1.2. Prewetting transition shifts to lower concentrations

Membrane binding not only affects the wetting transition line $\chi_b^*(\chi_{bm})$ but also changes the prewetting transition line (compare green line in figure 3(a) with figure 3(b)). These changes result from the fact that at the prewetting line not only c_s but also the area fraction of bound molecules ϕ_m is in general



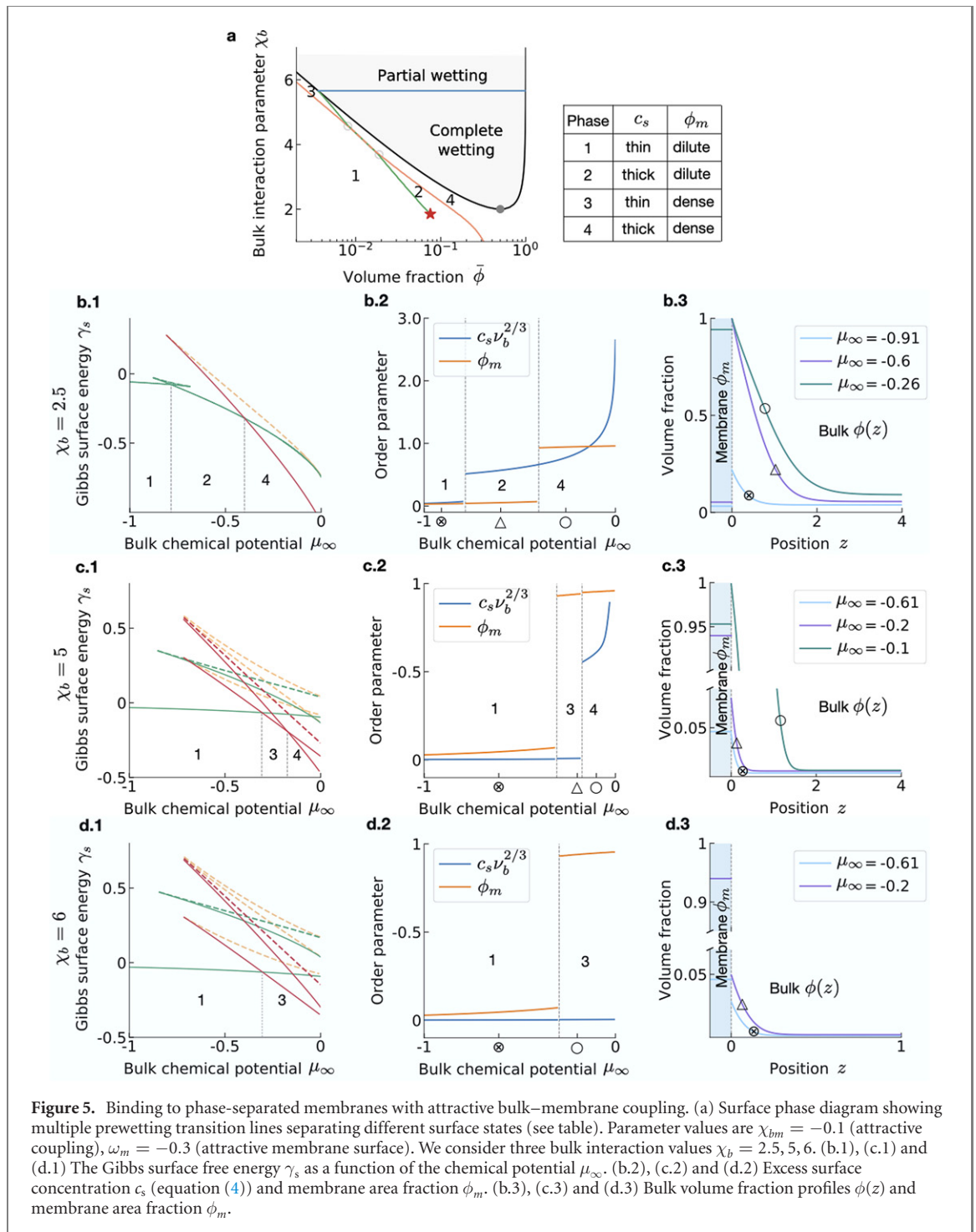
discontinuous (figure 4). In particular, since the prewetting line is linked to the wetting transition at the dilute branch of the binodal, the upshift of the wetting line for more attractive coupling also moves the prewetting line to smaller volume fractions ϕ . In addition, the critical point (red star) changes in a non-linear fashion with the coupling strength (figure 3(c)). Both trends significantly widen the prewetting regime (light red area), making the prewetting regime accessible for a broad range of interaction and coupling parameters. Interestingly, when the attractive coupling parameters is varied within a physically meaningful range in the order of a few $k_B T$, the volume fraction of the prewetting critical point can decrease by more than one order of magnitude (figures 3(e) and (f)). This implies that, due to binding, thick layers on the surface can already form via prewetting at bulk volume fraction far below the saturation concentration (compare red data points to binodal indicated by black line). Surprisingly, there is a minimum of critical volume fraction of the prewetting transition (figures 3(e) and (f)). This minimum arises because the critical values of the bulk interaction parameter χ_b also decrease for strongly attractive coupling strength χ_{bm} . A decreased bulk interaction parameter corresponds to interactions among bulk molecules becoming less attractive or even repulsive, in turn disfavoring the presence of bulk molecules adjacent to the membrane (inset, figure 3(f)). This also decreases the population of molecules bound to the surface ϕ_m (inset). We conclude that the minimal value of the critical prewetting volume fraction arises from a competition of the energy gain of molecules being bound and adjacent to the surface (favored for attractive coupling strength χ_{bm}) and the energy gain of molecules mixing with solvent in the bulk (favored by negative bulk interaction parameter χ_b corresponding to attractive solvent-molecule interactions).

3.1.3. Prewetting transition persists below the bulk critical point

In the absence of membrane binding, prewetting transitions can only occur for bulk interaction parameters above the bulk critical point where bulk phase separation is possible (gray dots are below the red star in figure 3(a)). The attractive coupling between bulk and membrane enables situations where the prewetting critical point shifts to values of bulk interaction parameter below the bulk critical point, where the bulk cannot phase-separate for any volume fraction ϕ (see domains separated by gray line, entitled ‘mixed bulk’ in figures 3(e) and (f)). In other words, binding mediates prewetting that is robust against concentration perturbations and that controls the formation of three-dimensional thick layers at surfaces, while phase separation in the bulk is suppressed. Similar findings were recently reported in experimental studies of functionalized surfaces and confirmed by corresponding Brownian dynamic simulations [32].

3.2. Wetting and prewetting with phase separation in the membrane

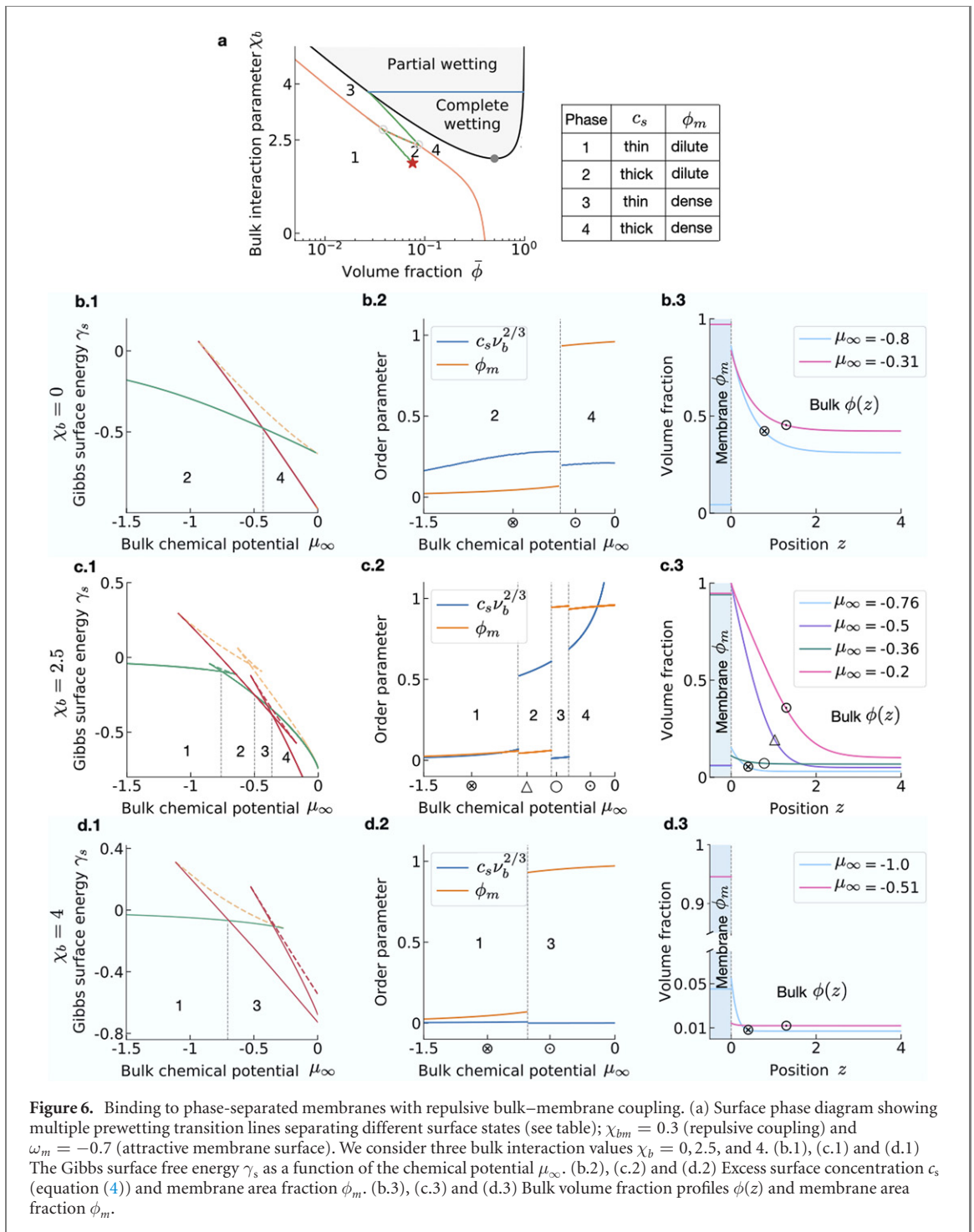
In this section, we will discuss how binding affects wetting and prewetting if molecules bound to the membrane can phase-separate. In other words, the membrane can undergo a surface phase transition independent of the bulk, which is realized by a positive interaction parameter $\chi_m > 2$ that characterizes the interactions among membrane-bound molecules. In the following, we choose $\chi_m = 3$. In our studies, we fix the coupling coefficients characterizing the interactions of bulk molecules with the surface, $\omega_b = -0.3$ and $\chi_{bb} = -0.5$. We vary the average volume fractions $\bar{\phi}$ and the bulk interaction parameter χ_b to calculate the corresponding surface phase diagrams. We discuss two choices for the coupling strength between membrane and bulk: an attractive interaction parameter $\chi_{bm} = -0.1$ and a repulsive one $\chi_{bm} = 0.3$, respectively. We find multiple striking effects on wetting and prewetting due to phase separation in membrane.



3.2.1. Phase transitions between four distinct surface states

When bound molecules can phase-separate in the membrane, wetting and prewetting transitions are affected due to the mutual coupling between membrane and bulk. This coupling is characterized by the coupling coefficient χ_{bm} , which links the behavior of the two respective order parameters ϕ_m and c_s . In general, we find that there are four types of thermodynamic states outside the domain of phase coexistence; see figures 5(a) and 6(a). These four surface states are the combinatoric possibilities between a thick or thin surface layer (high or low $c_s \nu_b^{2/3}$), and a dense or dilute phase of membrane-bound molecules (high or low ϕ_m). Similar to the case without phase separation of bound molecules in the membrane (figure 3(c)), such new thermodynamic prewetted states can be found in a broad range of bulk volume fractions and bulk interaction parameters.

In the surface phase diagrams, the four surface states are separated by first order phase transition lines at which, in general, both order parameters c_s and ϕ_m are discontinuous. The corresponding phase transitions



have mixed characteristics between a surface phase transition and a prewetting transition since bulk and membrane are coupled. However, we can test whether the transition lines exist for a decoupled bulk and membrane ($\chi_{bm} = 0$), and thus label surface phase transition lines (orange) and prewetting lines (green), separately. Due to the coupling, there can be phase transition lines that solely exist for a coupling between bulk and membrane (orange-green-dashed). Transition lines that intersect at triple points (light gray circles) at which three different surface states coexist; see figures 5(a) and 6(a).

The existence of multiple thermodynamic surface states can lead to complex Gibbs loops around the transition between two thermodynamic states. A classical Gibbs loop consists of two locally stable branches, which are connected by a locally unstable branch. To illustrate the Gibbs loop for prewetting transitions with membrane binding, we show the Gibbs surface energy γ_s as a function of the chemical potential of the reservoir, μ_∞ (figures 5(b.1), (c.1), (d.1) and 6(b.1), (c.1), (d.1)). At the phase transitions, the Gibbs surface energy of the thermodynamic state exhibits a kink, while the locally stable (solid lines) and unstable (dashed

lines) branches form the Gibbs loops. We find that the complexity of such Gibbs loops is different for different values of the bulk interaction χ_b . For example, we find classical Gibbs loops where two locally stable branches and one unstable branch exists in a certain chemical potential range of μ_∞ (figure 6(b1)). We also find cases where up to four locally stable surface states exists (figures 5(b.1), (c.1), (d.1) and 6(c.1), (d.1)). This structure of nested Gibbs loops suggest a complex dynamics toward equilibrium.

3.2.2. Correlated and anti-correlated jumps of surface order parameters

The sign of the discontinuity of both order parameters at the transition line is determined by whether the coupling is attractive ($\chi_{bm} < 0$) or repulsive ($\chi_{bm} > 0$). Specifically, for attractive couplings, both order parameters jump upwards as the chemical potential μ_∞ is increased, while for repulsive couplings, order parameters can show jumps in opposite directions; compare e.g. figures 5(c.2) and 6(c.2).

For attractive bulk–membrane couplings ($\chi_{bm} < 0$), and increasing chemical potential μ_∞ , either c_s or ϕ_m shows a pronounced jump upwards. This depends on the bulk interaction χ_b (compare figure 5(b.2) for $\chi_b = 2.5$ with figure 5(b.3) for $\chi_b = 5$). For more attractive bulk interactions ($\chi_b = 5$ versus $\chi_b = 2.5$), molecules prefer binding to accumulating at the membrane surface. Thus, the order parameters for membrane binding ϕ_m show the pronounced jump first as the chemical potential μ_∞ is increased (c.2), while for less attractive bulk interactions, the excess surface concentration c_s makes the bigger jump first (b.2). Thus, for the case of attractive bulk–membrane coupling, the layer width of the profile $\phi(z)$ as well as c_s increases for increasing μ_∞ (figures 5(b.3), (c.3) and (d.3)). In other words, the more molecules are in the bulk, the thicker the prewetted layer.

This behavior changes for the case of a repulsive bulk–membrane coupling ($\chi_{bm} > 0$). In this case, at each transition, both order parameters jump into opposite directions. Such opposite jumps can even cause a decrease in layer thickness of the profile $\phi(z)$ (figure 6(c.3)). Similar to the case of attractive couplings, the jump heights and the number of jumps depend on the bulk interactions χ_b (figures 6(b.2), (c.2) and (d.2)).

3.3. Wetting, prewetting and surface phase transitions with related bulk and surface interactions

In the last two sections we discussed wetting, prewetting and surface phase transitions for bulk interaction parameters χ_b and coupling parameters between bulk and membrane χ_{bm} that were varied independently from each other. However, if molecules that are bound to the membrane are the same as the molecules in the bulk, both parameters describe similar physical interactions and are therefore related. This relationship is specific to the system of interest and can depend on the membrane composition and the type of solvent and bulk molecule. To account for a relation between the interaction parameters χ_b and χ_{bm} , we consider for simplicity a linear relationship,

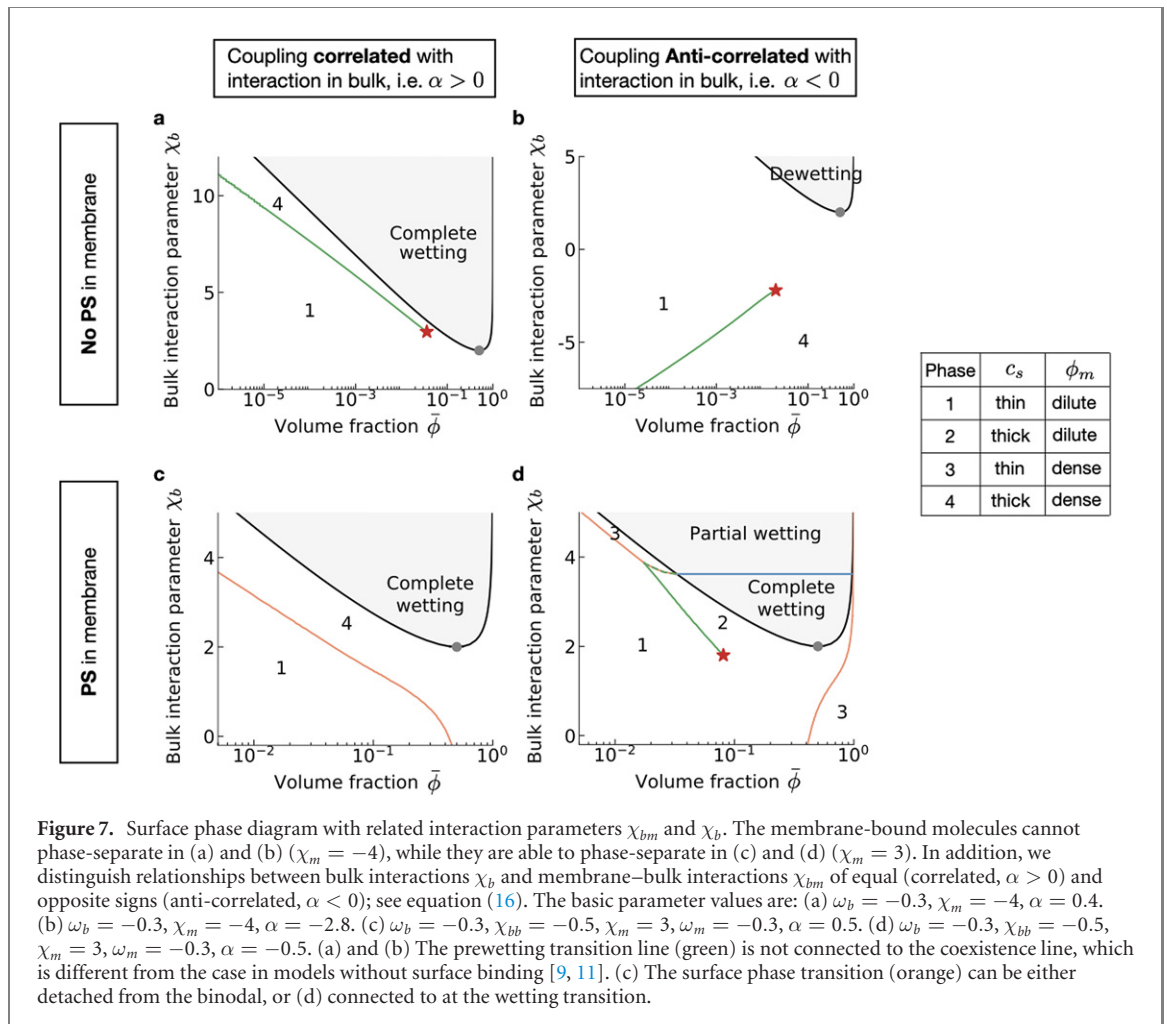
$$\chi_{bm} = -\alpha\chi_b, \quad (16)$$

where α describes the correlation between both interaction parameters. Interactions among bulk molecules and interaction of bulk with membrane-bound molecules can have equal ($\alpha > 0$) or opposite ($\alpha < 0$) signs, which we refer to the correlated and anti-correlated case, respectively. A positive α applies if interactions in the bulk are similar to interactions between bulk and bound molecules. A negative α could for example correspond to a situation where the molecular domain mediating the interactions in the bulk χ_b is also involved in binding to the surface and thus not accessible for interactions of bound molecules with bulk molecules χ_{bm} . For simplicity, the interaction parameter describing interactions among membrane-bound molecules χ_m is kept constant.

In the following, we study the phase diagrams of wetting, prewetting and surface phase transitions for correlated and anti-correlated interaction parameters. In addition, we distinguish between the cases with ($\chi_m = 3$) and without ($\chi_m = -4$) phase separation in the membrane. We find that the relation between interaction parameters χ_{bm} and χ_b (equation (16)) can lead to a rich plethora of phase diagrams with complex topologies of phase transition lines that qualitatively differ to results obtained from models without surface binding [9, 11]. For example, when molecules can bind to surfaces, prewetting transition lines can disconnect from the coexistence line, in particular from the wetting transition line (figures 7(a) and (b)). Thus, prewetted states can occur for a broad range of bulk interaction parameters χ_b . Furthermore, the wetting transition is suppressed such that either complete wetting (figure 7(a)) or dewetting (figure 7(b)) occurs inside the coexistence domain. Strikingly, the surface phase transition line is connected to the wetting transition (figure 7(d)). This implies that phase separation in the membrane-bound layer can control the transition between partial and complete wetted states (figure 7(d)).

3.3.1. Suppression of wetting transition

We first discuss the case of membrane-bound molecules that do not phase-separate in the membrane (e.g. $\chi_m = -4$). For correlated χ_b and χ_{bm} ($\alpha > 0$), partially wetted states are suppressed and complete wetting

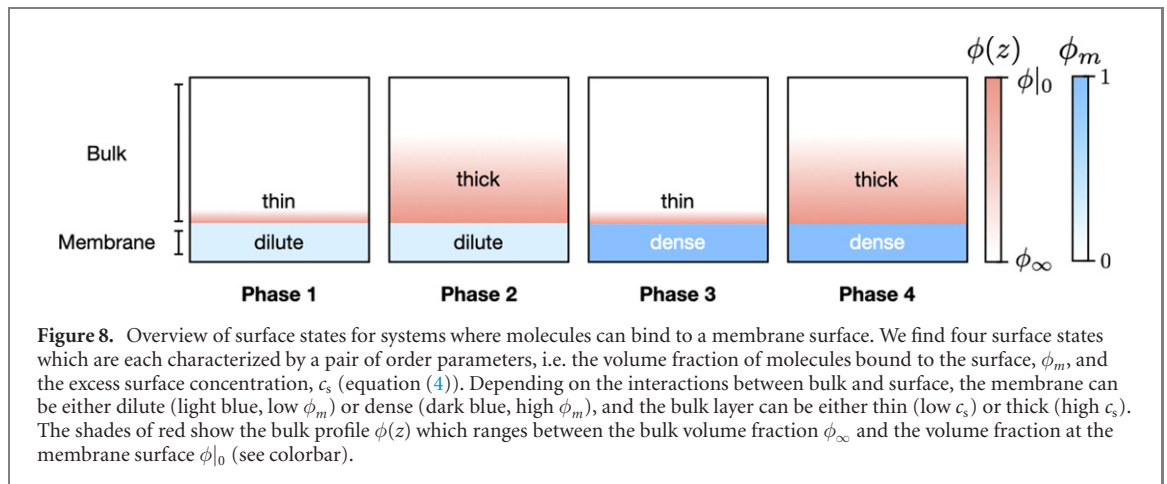


always occurs at coexistence regime (figure 7(a)). In this case, there is no wetting transition line and the prewetting line does not merge with the binodal. Moreover, the prewetting region where thick layers form enlarges for increasing bulk interaction parameter χ_b . The reason for the homogeneous states (completely wetted, thick layer) being favored on the membrane surface is that larger χ_b also implies more attractive bulk–membrane coupling ($\alpha > 0$). For anti-correlated χ_b and χ_{bm} ($\alpha < 0$), wetting can be completely suppressed for attractive bulk interactions ($\chi_b > 0$); see figure 7(b). In other words, within the coexistence regime, there are no condensates at the membrane surface. However, prewetted states can form for repulsive interactions among bulk molecules ($\chi_b < 0$). This case represents an ideal scenario to either prevent bulk condensates from interacting with surfaces or to enable prewetted condensates at surface without the capability of the bulk to form condensates.

Now we discuss the case where membrane-bound molecules can phase-separate in the membrane (e.g. $\chi_m = 3$). If χ_b and χ_{bm} are correlated ($\alpha > 0$), complete wetting is favored over partial wetting in the coexistence regime (figure 7(c)), similar to the case without phase separation in the membrane (figure 7(a)). Also, the domain of surface states broadens as the bulk interaction parameters get more attractive. The only qualitative difference to the case without phase separation in the membrane is that there is no critical point of prewetting (figure 7(c)). The reason is that though both, bulk interactions (negative χ_b) and membrane–bulk interactions get more repulsive, the ability to phase-separate in the membrane can still enable thick layers at the membrane surface.

3.3.2. Phase separation in membrane facilitates wetting

With independent interaction parameters χ_b and χ_{bm} (see figures 5(a) and 6(a)), the surface phase transition (orange lines) does not intersect with the binodal while the prewetting transition line (green lines) merges tangentially. The latter is also the case in model without membrane binding [9, 11]. However, for anti-correlated χ_b and χ_{bm} ($\alpha < 0$) and phase separation in the membrane (figure 7(d)), the surface phase transition intersects with the binodal line at the wetting transition. This finding indicates that membrane-bound molecules coupled to the bulk can alter the interplay between wetting and prewetting



transition. Furthermore, for strongly attractive bulk interactions (large χ_b) prewetting can even occur at conditions below the bulk critical point mediated by phase separation in the membrane. Finally, the membrane phase transition in the absence of bulk interactions (e.g. $\chi_b = 0$) is now disconnected from the prewetting lines but converges to the binodal of the dense phase (figure 7(d)).

3.3.3. Antagonism between membrane-bound and prewetted layers

In classical wetting and prewetting (figure 3(a)), the profile of a thick layer curves upwards when approaching the surface due to attractive interactions between bulk and surface ($\omega_b < 0$). In the presence of membrane binding this leads to a high area fraction ϕ_m in the membrane for correlated interaction parameters ($\alpha > 0$). This situation can fundamentally change when membrane binding and prewetting are antagonistic due to anti-correlated interaction parameters ($\alpha < 0$). As a result of this anti-correlation, we can distinguish between two types of antagonistic cases. First, a thick prewetting layer near the surface can induce detachment of molecules from the surface (purple lines in figure 9(d)). Molecules cannot bind to the surface and thus the surface is effectively attractive. Second, molecules bind to the membrane surface which thereby becomes repulsive for bulk molecules. No prewetting layer forms and the concentration profile even curves downward when approaching the surface (see figure 9(d)).

4. Discussion

Due to the significance of both binding processes and bulk condensation in living cells we study how membrane binding affects wetting, prewetting and surface phase transitions. To approach this question, we derive the corresponding thermodynamic theory in the presence of binding processes of molecules between bulk and membrane surfaces. Our theory goes beyond the classical thermodynamics of phase transitions at and adjacent to surfaces by introducing new surface states. Recently, related questions were addressed using Monte-Carlo simulations of a ternary lattice model for mobile tethers that are confined in a membrane and that can bind bulk molecules [33]. This work focuses on the role of three phase coexistence in the membrane while all the molecules in this model are constituents of the bulk domain.

In our theory we focus on a binary mixture in the bulk that interacts with a surface layer bound to a flat and rigid membrane. The molecules can exchange between bulk and membrane domains via binding and unbinding processes. Our thermodynamic theory shows that membrane binding can lead to a variety of thermodynamic surface states at undersaturated conditions with unexpectedly rich surface phase diagrams (see figure 8). Such states are described by a pair of order parameters, i.e. the area fraction of bound molecules in a single surface layer and the excess surface concentration of the condensates adjacent to the surface. Interestingly, we find cases where phase transitions at and adjacent to surfaces occur under conditions where the bulk cannot phase-separate at any concentration. More generally, a layer of bound molecules on the membrane effectively modifies the properties of the surface which can for example lead to a shift of the prewetting line to low concentrations. Finally, surface binding affects the wetting transition and the contact angle of bulk droplets that wet the surface.

Our findings additionally suggest that the binding of molecules provides a versatile mechanism to control the position of wetted droplets at phase coexistence. In recent years, a growing number of intra-cellular condensates were shown to adhere to membrane-bound organelles or the intra-cellular surfaces [2, 7, 8, 24, 34]. Moreover, many of such condensates are suggested to act as scaffolds for

biochemical processes [35, 36]. Specific binding receptors at the membrane surface can control the position of such wetted droplets and thereby spatially control biological processes occurring inside droplets.

We also find that binding alters the prewetting behavior and the occurrence of surface phase transitions at concentrations below saturation. Since molecules can bind to the membrane surfaces, phase-separation can occur in the membrane (surface phase transition) altering the prewetting behavior by effectively modifying the properties of the surface. Moreover, while the classical prewetting transition line is very close to the saturation concentration without binding processes ([21, 37]; see also figure 3(a)), the transition lines of prewetting and surface phase transitions can shift to lower values when molecules can bind to membrane surfaces. Interestingly, the actual physiological concentrations of many membrane-binding proteins in living cells (typically (10–100) nM [22–24, 38]) are far below their saturation concentrations (typically (1–10) μ M [24, 34]). Further research is required to scrutinize whether the low physiological concentrations of membrane-binding proteins serve the purpose to form condensates on intracellular surfaces rather than droplets in the bulk.

Returning to Pauli's famous quote, surfaces in biological systems were probably not invented by the devil. Rather, membranes and surfaces have an essential functional role for living cells. This essential role is reflected in a plethora of biological processes ranging from cell division to intra- and extra-cellular transport. Binding to such surfaces together with surface phase transitions gives rise to a new level of complexity that is exemplified in the rich variety of phases and variability of phase diagrams revealed by our work. This suggests that this additional complexity could play a key role in cell biological processes. We expect that this complexity is further extended when orientations of surface bound molecules can give rise to nematic phases [39]. Complex patterns at surface are expected when binding processes are maintained away from thermodynamic equilibrium, which is the case in living cells. In biological systems, ATP-driven cycles of kinase and phosphatase can alter binding equilibria. Future research will clarify how such active binding processes modify the properties of wetted and prewetted states out of equilibrium.

Acknowledgments

We thank S Liese, J Bauermann, L Hubatsch, S Bo, S Laha, T Harmon, I LuValle-Burke, and D Sun for insightful discussions and S Liese for helpful feedback on the manuscript. G Bartolucci, A Honigmann, and C Weber acknowledge the SPP 2191 'Molecular Mechanisms of Functional Phase Separation' of the German Science Foundation for financial support and for providing an excellent collaborative environment.

Data availability statement

No new experimental data were created or analysed in this study.

Appendix A. Graphical construction for surface phase transitions with membrane binding

Equation (9) are one differential equation of second order for the bulk volume fraction $\phi(z)$ coupled to three algebraic equations at the membrane boundary and at $z \rightarrow \infty$. In this section, we integrate once, leading to a differential equation of first order coupled to two algebraic equations. The resulting set of equations can then be solved by a graphical construction, a procedure which is similar to reference [9].

After multiplying equation (9a) by $(\partial\phi/\partial z)$ on both sides, one obtains

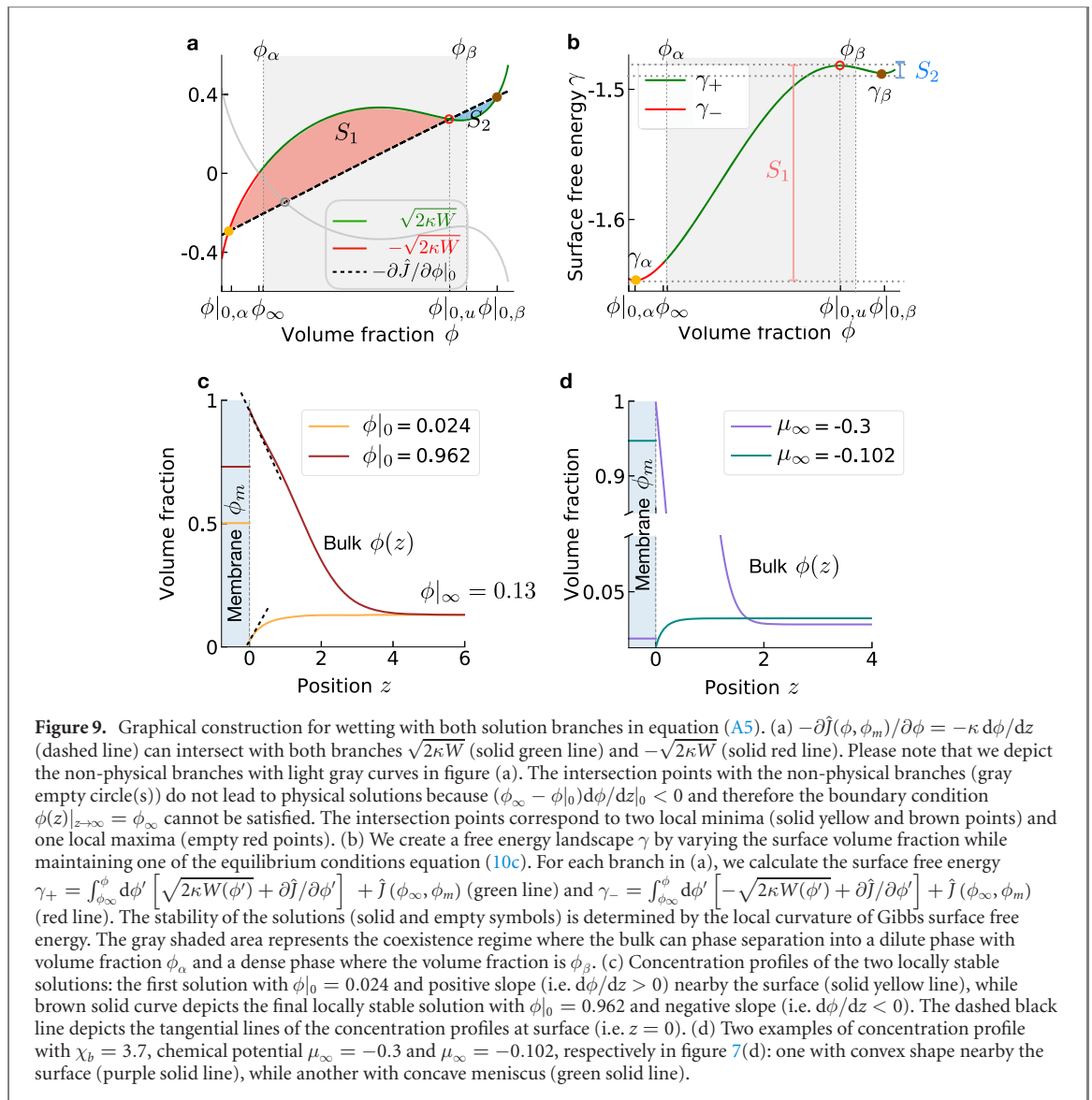
$$\frac{\partial f_b}{\partial z} - \frac{1}{\nu_b} \mu_\infty \frac{\partial \phi}{\partial z} - \frac{\partial}{\partial z} \left(\frac{\kappa}{2} (\partial_z \phi)^2 \right) = 0. \quad (\text{A1})$$

Integrating this equation over the bulk,

$$\int_z^\infty dz' \left[\frac{\partial f_b}{\partial z'} - \frac{1}{\nu_b} \mu_\infty \frac{\partial \phi}{\partial z'} - \frac{\partial}{\partial z'} \left(\frac{\kappa}{2} (\partial_{z'} \phi)^2 \right) \right] = 0, \quad (\text{A2})$$

and utilising boundary conditions $\partial_z \phi|_\infty = 0$ (equation (9b)), and $\phi(\infty) = \phi_\infty$, we obtain

$$0 = f_b(\phi(z)) - f_b(\phi_\infty) - \mu_\infty \left(\frac{1}{\nu_b} \phi(z) - \frac{1}{\nu_b} \phi_\infty \right) - \frac{\kappa}{2} (\partial_z \phi)^2. \quad (\text{A3})$$



Using the definition of $W(\phi)$ (equation (10d)), equation (A3) can be written as

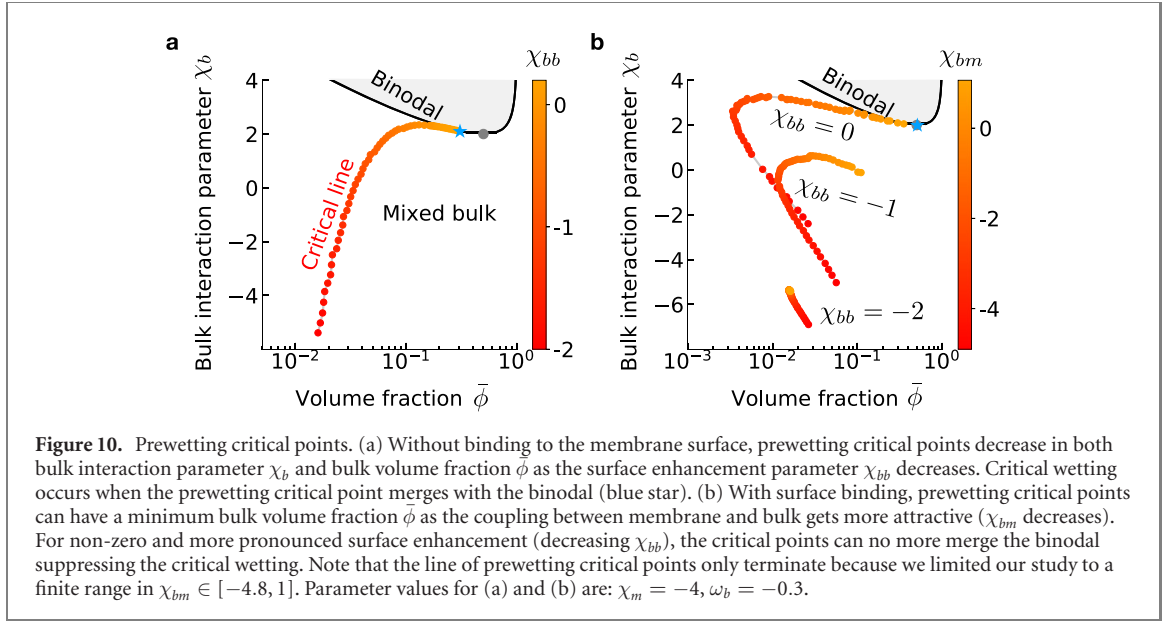
$$|\partial_z \phi|^2 = \frac{2}{\kappa} W(\phi), \quad (\text{A4})$$

leading to two solution branches (red and green lines in figure 9):

$$\partial_z \phi = \pm \sqrt{\frac{2}{\kappa} W(\phi)}. \quad (\text{A5})$$

Finally, substituting these two relations into equation (9c), we obtain equation (10b). Please note that since we have already used equation (9b) in the derivation above, we are left with two algebraic equations and one ODE of first order (see equation (10)). These equations can be solved via a graphical construction to obtain the surface volume fraction $\phi|_0$ and membrane area fraction ϕ_m at thermodynamic equilibrium; see figure 9 for an illustration in the presence of the two solution branches (equation (A5)).

Numerical methods to obtain solutions to equation (10) may suffer from the fact that the bulk chemical potential $\mu_b = \partial f_b / \partial \phi$ is singular for $\phi = 1$. To avoid numerical problems related to this singularity, we can add a term of the form $-\epsilon(1 - \phi)\ln(1 - \phi)$ to the coupling free energy J such that $-\partial J / \partial \phi|_0$ can always intersect with $\sqrt{2\kappa W}$ in the limit $\phi \rightarrow 1$. We used $\epsilon = 10^{-3}$, which is a very small number to ensure that the thermodynamic states are hardly affected.



Appendix B. Condition of critical prewetting

In this section, we derive the condition for prewetting critical points with membrane binding. At the prewetting critical point, the Gibbs surface potential $\gamma_s(\phi|_0)$ given in equation (11) has a zero curvature with respect to $\phi|_0$,

$$\frac{\kappa W'(\phi|_0)}{\sqrt{2\kappa W(\phi|_0)}} \pm \frac{\partial^2 J(\phi, \phi_m)}{\partial \phi^2} \Big|_0 \pm \frac{\partial^2 J(\phi, \phi_m)}{\partial \phi \partial \phi_m} \frac{\partial \phi_m}{\partial \phi} \Big|_0 = 0, \quad (\text{B1})$$

where $\partial \phi_m / \partial \phi|_0$ can be obtained from the derivative of equation (10c):

$$\frac{\partial^2 f_m}{\partial \phi_m^2} \frac{\partial \phi_m}{\partial \phi} \Big|_0 + \frac{\partial^2 J(\phi, \phi_m)}{\partial \phi_m^2} \frac{\partial \phi_m}{\partial \phi} \Big|_0 + \frac{\partial^2 J(\phi, \phi_m)}{\partial \phi_m \partial \phi} \Big|_0 = 0. \quad (\text{B2})$$

Substituting $J(\phi, \phi_m)$ given in equation (15c) and f_m given in equation (15), we obtain

$$\frac{\partial \phi_m}{\partial \phi} \Big|_0 = \chi_{bm} \frac{\phi_m(1 - \phi_m)}{(1 - 2\chi_m \phi_m(1 - \phi_m))}. \quad (\text{B3})$$

Combining equation (B1) with equation (B3), we find the condition for prewetting critical point,

$$\sqrt{\frac{\kappa}{2W(\phi)}} \frac{\tilde{\nu}}{\nu_b} \left[\ln \phi - n_b \ln(1 - \phi) + n_b \chi_b(1 - 2\phi) - \frac{\mu_\infty}{k_B T} \right] \pm \left[\chi_{bb} + \chi_{bm}^2 \frac{\phi_m(1 - \phi_m)}{(1 - 2\chi_m \phi_m(1 - \phi_m))} \right] = 0, \quad (\text{B4})$$

where $W(\phi)$ is defined in equation (10d).

Appendix C. Comparison with Nakanishi and Fisher's results

In this section, we compare our results with Nakanishi and Fisher's results [11]. We distinguish two scenarios in the following discussion: with and without phase separation in the membrane-bound layer. If the membrane-bound layer cannot phase-separate (i.e. $\chi_m < 2$ for $n_m = 1$), the terms in the coupling free energy, $\chi_{bm} \phi_m \phi_s$, and $\chi_{bb} \phi^2$ can both act as an effective surface enhancement for $\chi_{bm} < 0$ and $\chi_{bb} < 0$. Here, we scrutinize whether the effects of the coupling parameter χ_{bm} are indeed qualitatively similar to the ones of the classical enhancement parameter χ_{bb} as analyzed previous models [9, 11]. In figure 10, we show a $\chi_b - \bar{\phi}$ phase diagrams and depict the critical prewetting points, (a) for the case without binding when varying χ_{bb} , and (b) for the case with membrane binding as a function of the coupling parameter χ_{bm} for $\chi_{bb} = 0$. We find that both cases share a similarity, namely when decreasing χ_{bb} for the case without binding or decreasing χ_{bm} for the case with binding, the prewetting points shift to lower bulk interaction parameters χ_b . However, both cases also show qualitative differences. First, for the case without binding, the

critical points shift to lower bulk volume fraction $\bar{\phi}$, while there is a minimum in $\bar{\phi}$ for the case with binding. Second, without binding, there is a χ_{bb} value where the prewetting critical point coincides with the binodal line implying a continuous wetting transition as reported in reference [11]. This is different to the case with surface binding and $\chi_{bb} = 0$, where the prewetting critical point merges with the bulk critical point, thereby fusing bulk and surface criticality. For non-vanishing surface enhancement, e.g. $\chi_{bb} = -1$, critical wetting is even suppressed for the case with binding since the critical prewetting line remains disconnected from the binodal for any coupling parameters χ_{bm} . Furthermore, positive coupling coefficient χ_{bm} can never lead to critical wetting transition for any value $\chi_{bb} \leq 0$. However, for positive surface enhancement $\chi_{bb} > 0$, critical wetting can occur in our model. In summary, in the absence of phase separation in the membrane, the case with and without binding leads to a qualitative different thermodynamic behavior at surface.

If the membrane-bound layer can phase-separate (i.e. $\chi_m > 2$ for $n_m = 1$), the case with and without binding leads even more qualitative differences. For example, we obtain multiple surface states (see figures 5(a) and 6(a)), which can not be obtained from Nakanishi and Fisher's results. Furthermore, if we consider a relationship between the interaction parameters χ_{bm} and χ_b e.g. equation (16), we find prewetting transition lines which are not connected with coexistence line (see figures 7(a) and (b)).

ORCID iDs

Alf Honigmann  <https://orcid.org/0000-0003-0475-3790>

Frank Jülicher  <https://orcid.org/0000-0003-4731-9185>

Christoph A Weber  <https://orcid.org/0000-0001-6279-0405>

References

- [1] Jamtveit B and Meakin P 1999 *Growth, Dissolution and Geosystems* (Berlin: Springer) p 291
- [2] Brangwynne C P, Eckmann C R, Courson D S, Rybarska A, Hoege C, Gharakhani J, Jülicher F and Hyman A A 2009 Germline p granules are liquid droplets that localize by controlled dissolution/condensation *Science* **324** 1729–32
- [3] Hyman A A, Weber C A and Jülicher F 2014 Liquid–liquid phase separation in biology *Annu. Rev. Cell Dev. Biol.* **30** 39–58
- [4] Banani S F, Lee H O, Hyman A A and Rosen M K 2017 Biomolecular condensates: organizers of cellular biochemistry *Nat. Rev. Mol. Cell Biol.* **18** 285–98
- [5] Brangwynne C P, Mitchison T J and Hyman A A 2011 Active liquid-like behavior of nucleoli determines their size and shape in *xenopus laevis* oocytes *Proc. Natl Acad. Sci.* **108** 4334–9
- [6] Feric M, Vaidya N, Harmon T S, Mitrea D M, Zhu L, Richardson T M, Kriwacki R W, Pappu R V and Brangwynne C P 2016 Coexisting liquid phases underlie nucleolar subcompartments *Cell* **165** 1686–97
- [7] Gall J G, Bellini M, Wu Z and Murphy C 1999 Assembly of the nuclear transcription and processing machinery: Cajal bodies (coiled bodies) and transcriptosomes *Mol. Biol. Cell* **10** 4385–402
- [8] Agudo-Canalejo J et al 2021 Wetting regulates autophagy of phase-separated compartments and the cytosol *Nature* **591** 142–6
- [9] Cahn J W 1977 Critical point wetting *J. Chem. Phys.* **66** 3667–72
- [10] Ebner C and Saam W F 1977 New phase-transition phenomena in thin argon films *Phys. Rev. Lett.* **38** 1486–9
- [11] Nakanishi H and Fisher M E 1982 Multicriticality of wetting, prewetting, and surface transitions *Phys. Rev. Lett.* **49** 1565–8
- [12] de Gennes P G 1985 Wetting: statics and dynamics *Rev. Mod. Phys.* **57** 827–63
- [13] Diehl H W and Dietrich S 1985 *Static and Dynamic Critical Behavior at Surfaces* (Berlin: Springer) pp 39–52
- [14] Gelfand M P and Lipowsky R 1987 Wetting on cylinders and spheres *Phys. Rev. B* **36** 8725–35
- [15] Diehl H W 1997 The theory of boundary critical phenomena *Int. J. Mod. Phys. B* **11** 3503–23
- [16] Bonn D, Eggers J, Indekeu J, Meunier J and Rolley E 2009 Wetting and spreading *Rev. Mod. Phys.* **81** 739–805
- [17] Lipowsky R 2018 Response of membranes and vesicles to capillary forces arising from aqueous two-phase systems and water-in-water droplets *J. Phys. Chem. B* **122** 3572–86
- [18] Napiórkowski M, Schimmele L and Dietrich S 2020 Wetting transitions on soft substrates *Europhys. Lett.* **129** 16002
- [19] Rutledge J E and Taborek P 1992 Prewetting phase diagram of ^4He on cesium *Phys. Rev. Lett.* **69** 937
- [20] Chandavarkar S, Geertman R M and de Jeu W H 1992 Observation of a prewetting transition during surface melting of caprolactam *Phys. Rev. Lett.* **69** 2384–7
- [21] Kellay H, Bonn D and Meunier J 1993 Prewetting in a binary liquid mixture *Phys. Rev. Lett.* **71** 2607
- [22] Banjade S and Rosen M K 2014 Phase transitions of multivalent proteins can promote clustering of membrane receptors *Elife* **3** e04123
- [23] Su X et al 2016 Phase separation of signaling molecules promotes T cell receptor signal transduction *Science* **352** 595–9
- [24] Beutel O, Maraspin R, Pombo-García K, Martin-Lemaitre C and Honigmann A 2019 Phase separation of zonula occludens proteins drives formation of tight junctions *Cell* **179** 923–36
- [25] Loose M, Fischer-Friedrich E, Ries J, Kruse K and Schwille P 2008 Spatial regulators for bacterial cell division self-organize into surface waves *in vitro Science* **320** 789–92
- [26] Halatek J and Frey E 2012 Highly canalized mind transfer and mine sequestration explain the origin of robust mincde-protein dynamics *Cell Rep.* **1** 741–52
- [27] Ramm B, Heermann T and Schwille P 2019 The E. coli mincde system in the regulation of protein patterns and gradients *Cell. Mol. Life Sci.* **76** 4245–73
- [28] Schwayer C, Shamipour S, Pranjic-Ferscha K, Schauer A, Balda M, Tada M, Matter K and Heisenberg C-P 2019 Mechanosensation of tight junctions depends on Zo-1 phase separation and flow *Cell* **179** 937–52

- [29] Quail T, Golfier S, Elsner M, Ishihara K, Jülicher F and Brugués J 2020 Capillary forces drive pioneer transcription factor-mediated DNA condensation *bioRxiv Preprint* <https://doi.org/10.1101/2020.09.17.302299> (accessed 20 September 2020)
- [30] Morin J A, Wittmann S, Choubey S, Klosin A, Golfier S, Hyman A A, Jülicher F and Grill S W 2020 Surface condensation of a pioneer transcription factor on DNA *bioRxiv Preprint* <https://doi.org/10.1101/2020.09.24.311712> (accessed 25 September 2020)
- [31] Snead W T and Gladfelter A S 2019 The control centers of biomolecular phase separation: how membrane surfaces, PTMs, and active processes regulate condensation *Mol. Cell* **76** 295–305
- [32] Jana P K and Moggetti B M 2019 Surface-triggered cascade reactions between DNA linkers direct the self-assembly of colloidal crystals of controllable thickness *Nanoscale* **11** 5450–9
- [33] Rouches M, Veatch S and Machta B 2021 Surface densities prewet a near-critical membrane *Proceedings of the National Academy of Sciences* **118** 40
- [34] Liu Z *et al* 2020 Par complex cluster formation mediated by phase separation *Nat. Commun.* **11** 2266
- [35] Boeynaems S *et al* 2018 Protein phase separation: a new phase in cell biology *Trends Cell Biol.* **28** 420–35
- [36] Alberti S, Gladfelter A and Mittag T 2019 Considerations and challenges in studying liquid–liquid phase separation and biomolecular condensates *Cell* **176** 419–34
- [37] Schmidt J W and Moldover M R 1983 First-order wetting transition at a liquid–vapor interface *J. Chem. Phys.* **79** 379–87
- [38] Goehring N W, Trong P K, Bois J S, Chowdhury D, Nicola E M, Hyman A A and Grill S W 2011 Polarization of par proteins by advective triggering of a pattern-forming system *Science* **334** 1137–41
- [39] Milchev A and Binder K 2021 Cylindrical confinement of solutions containing semiflexible macromolecules: surface-induced nematic order versus phase separation *Soft Matter* **17** 3443–54